Measuring thermal conductivity of nanostructures with the 3ω method: the need for finite element modeling

To cite this article: Lorenzo Peri *et al* 2023 *Nanotechnology* **34** 435403

View the article online for updates and enhancements.

IOP Publishing

Measuring thermal conductivity of nanostructures with the 3ω method: the need for finite element modeling

Lorenzo Peri[1,2]**, Domenic Prete**[3] **, Valeria Demontis**[3]**, Elena Degoli**[4]**, Alice Ruini**[5]**, Rita Magri**[5] **and Francesco Rossella**[5]

[1] Cavendish Laboratory, University of Cambridge, J.J. Thomson Avenue, Cambridge CB3 0HE, United Kingdom
[2] Quantum Motion, 9 Sterling Way, London N7 9HJ, United Kingdom
[3] NEST, Scuola Normale Superiore and Istituto Nanoscienze-CNR, Piazza S. Silvestro, 12, 56127, Pisa, Italy
[4] Dipartimento di Scienze e Metodi dell'Ingegneria, Università di Modena e Reggio Emilia, Modena, Italy
[5] Dipartimento di Scienze Fisiche, Informatiche e Matematiche, Università di Modena e Reggio Emilia, Modena, Italy

E-mail: domenic.prete@sns.it

CrossMark

Abstract

Conventional techniques of measuring thermal transport properties may be unreliable or unwieldy when applied to nanostructures. However, a simple, all-electrical technique is available for all samples featuring high-aspect-ratio: the 3ω method. Nonetheless, its usual formulation relies on simple analytical results which may break down in real experimental conditions. In this work we clarify these limits and quantify them via adimensional numbers and present a more accurate, numerical solution to the 3ω problem based on the Finite Element Method (FEM). Finally, we present a comparison of the two methods on experimental datasets from InAsSb nanostructures with different thermal transport properties, to stress the crucial need of a FEM counterpart to 3ω measurements in nanostructures with low thermal conductivity.

Supplementary material for this article is available online

Keywords: 3ω method, finite element analysis, energy harvesting, low K materials, thermoelectricity, thermal conductivity measurement

(Some figures may appear in colour only in the online journal)

1. Introduction

The urgent need for energy sources in novel devices, such as wearables or biomedicals, has boosted the interest in the field of nanostructure development for thermoelectric applications. This entails the generation of a potential difference arising from a temperature gradient, which can be used to locally harness energy to power devices of interest. The thermoelectric performance of a specimen can be shown to depend on an adimensional quantity, named the thermoelectric figure of merit, which depends on the ratio between the electric and thermal conductivity of the material chosen for the thermoelectric device. The recently-demonstrated ability to engineer semiconducting nanowires (NWs) to lower their thermal conductivity without affecting their electrical transport properties [1–7]—a promising feature coming from phonon scattering with the boundaries of the nanostructure, i.e. the Casimir effect [8]—has made them an extremely interesting platform to realize high room-temperature figures of merit, to rival those of more-established industry standard thermoelectric materials (e.g. Bi_2Te_3) [9, 10]. Because of the promising results that have been achieved in this regard, it is of capital importance to have a simple and reliable method to measure the thermal transport properties of such nanostructures
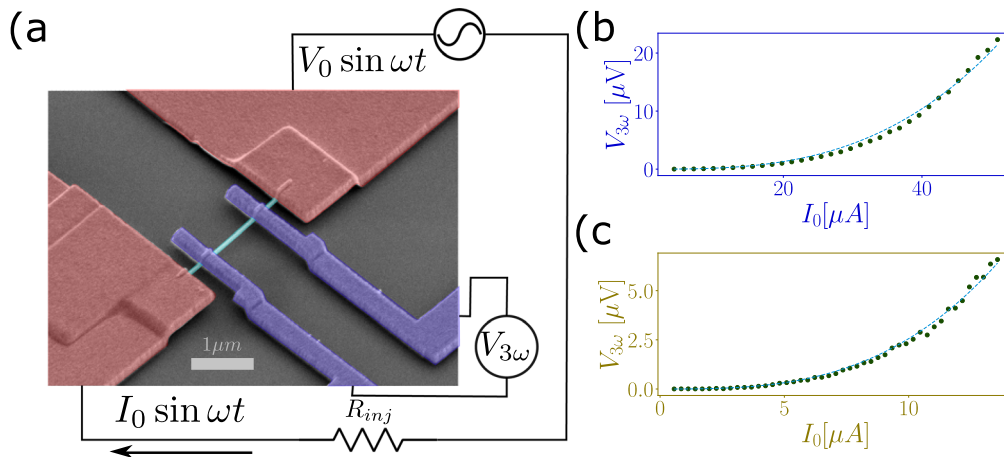
Figure 1. (a) Typical setup for a 3ω measurement, with a suspended NW connected to a 4-probe setup. An AC injection current $I_0 \sin(\omega t)$ is forced through the nanostructure via the outer pads, that also serve as thermal anchoring, while the third harmonic of the voltage drop is measured by a Lock-In amplifier. (b)–(c) Typical measures and best-fit for two InAsSb NWs, one with a single-crystal zincblende crystal structure (c), the other with an engineered nanostructure to reduce thermal conductivity (b). The model of the best fit and its validity are discussed at length in section 2. Data taken as described in [2]

[11, 12]. Among the others, the 3ω method, an all-electrical measurement technique of the thermal conductivity, has gained particular interest [13–18]. The particular appeal of this technique resides in its ease of application to a suspended NW, not requiring the use of optical setups [19, 20] or the use of externally-applied temperature gradients [21–23].

In this work, we shall discuss the underlying theory to the 3ω method, commenting on the simple analytical solution presented in [24] obtained under certain approximations. We shall moreover discuss said approximations, and their break down in common experimental conditions, e.g. for samples featuring extremely low thermal conductivities. We then clarify these limits and easily quantify them via adimensional numbers. From these observations, we shall detail the need in said cases of a more accurate, i.e. numerical, treatment of the problem, which we describe in the form of Finite Element Modelling [25–30]. Finally, we shall employ both methods on experimental data from InAsSb Nws to show up to a 40% underestimation of the thermal conductivity when the analytical formula framework is employed, compared to its numerical counterpart.

We shall stress how all the results derived in this work are trivially generalised to any high-aspect-ratio nanostructure. Thus, we believe this work provides an extensive proof of the limits of the conventionally employed 3ω technique coupled with the analytical model and provides an effective solution to overcome its limitations, paving the way for more robust and accurate measurements of the ever-increasing thermoelectric performance of engineered nanostructures with progressively lower thermal conductivities.

The two larger outside pads are used for feeding the AC current I and double as a thermal anchor for the NW allowing to minimize any temperature rise owing to the metal/semiconductor thermal contact resistance thanks to the maximization of the NW/metal contact area, while the smaller inner contacts act as voltage probes to measure the voltage drop across the specimen. The whole NW is suspended to avoid thermal conduction between the specimen and the substrate, which introduces major detrimental effects on the measurement of NW thermal conductivity [31]. The system is also in a vacuum, thus thermal dissipation in the form of convection between the specimen and the surrounding air shall not be considered in this work.

The first harmonic is used to measure the NW electrical resistance R_0 at the starting temperature T_0 according to Ohm's Law, while the third harmonic can be related to the thermal conductivity κ of the NW, as described in the following.

All measurements are generally performed with a Lock-In amplifier, generating an AC voltage $V_0 \sin \omega t$. As shown in figure 1(a), a constant injection current is maintained by connecting the NW in series with an injection resistance $R_{inj} \gg R_0$. This is required so that the majority of the voltage drop occurs across R_{inj}, and the amplitude I_0 can be approximated to V_0/R_{inj}, which is independent of the NW resistance. Noticeably, this assumption generally holds true for the materials of interest for the exploitation of thermoelectric effects, i.e. materials featuring good electrical transport properties coupled with poor thermal transport properties. Furthermore, a high electrical conductivity is also auspicial for the 3ω measurement itself, since it allows for easier measurement of the third harmonic signal.

2. Method

The 3ω method is based on the injection of an AC current and the measurement of the first and third harmonic of the voltage drop across the NW, hence the name 3ω. A typical setup to perform this measurement on a NW is depicted in figure 1(a).

3. Results

3.1. Theory of the 3ω problem

In the subsequent sections we shall briefly retrace the analytical approach to the 3ω method as presented in [24], to
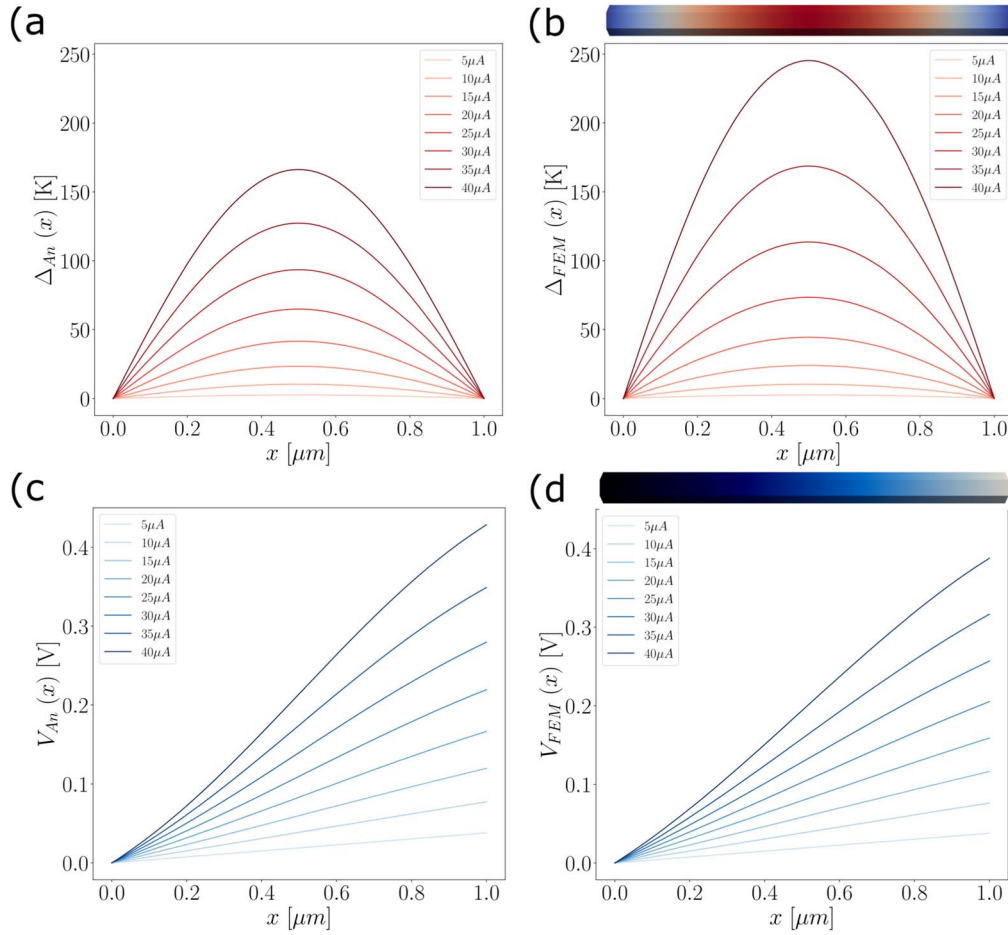
Figure 2. Comparison between the analytical (left) and FEM (right) RMS temperature and voltage profiles in the case of an InAsSb NW with 1 μm length, 35 nm diameter, and $\kappa = 1.5\frac{W}{mK}$. Comparing panels (a)–(b) we can see how the two models are in qualitative agreement, and predict comparable $\Delta(x)$ for low injection currents (legend). At larger currents , however, the low κ makes Θ increase significantly, reaching $\Theta = 0.33$ for the higher value. Thus, The analytical approach is no longer valid, and it significantly underestimates the peak temperature. This results in different Voltage profiles, as clear comparing panels (c)–(d). On the FEM simulations, we report also an example of the false-color solution across the whole mesh, to highlight the translational invariance in $\hat{y}$ and $\hat{z}$.

introduce the relevant physical quantities and adimensional transport numbers. This will allow for a discussion of the inherent limitations of the often-used analytical treatment, and highlight the approximations which can be lifted via a Finite Element Modelling (FEM) approach.

3.2. Analytical model

The core of this nonlinear phenomenon is the dependency of the NW electrical with temperature, which is in turn raised by the injection current via the Joule effect. For simplicity of modelling, we posit that the NW resistance is linear with the temperature change

$$R(T) = R_0 + R'(T - T_0), \qquad (1)$$

where we have defined $R' = \frac{dR}{dT}$, assumed constant in the whole range of temperatures of interest. T_0 is a fixed reference temperature at which the system is assumed to be in equilibrium when unperturbed, and $R_0 = R(T_0)$ is the electrical resistance of the specimen at $T = T_0$. Considering an injection current $I(t) = I_0 \sin(\omega t)$, the partial differential equation

(PDE) governing the local NW temperature reads

$$\rho C_p \frac{\partial}{\partial t} T(\vec{x}, t) - \kappa \nabla^2 T(\vec{x}, t)$$
$$= \frac{I_0^2 \sin^2(\omega t)}{LS}(R_0 + R'(T(\vec{x}, t) - T_0)), \qquad (2)$$

where ρ is the density of the material, C_p it is specific heat at constant pressure, κ is the thermal conductivity, and L, and S are the NW length and cross-section respectively.

For ease of future notation during, it is best to define the current density $j_0 = \frac{I_0}{S}$ and the electrical resistivity $\rho_{el} = R\frac{L}{S}$, so that $\rho'_{el} = \frac{d}{dT}\rho_{el}$.

Equation (2), together with the appropriate boundary conditions, completely describes the physics of our system. However, it is important here to note that this is still a 3D problem in $\vec{x}$, which does not possess a simple analytical solution for the rather complex NW geometry. Nevertheless, we can easily simplify the treatment by noting that, by virtue of neglecting gas convection and black-body radiation [32], as well as suspending the NW to thermally decouple it from the substrate, there are no physical processes occurring at the
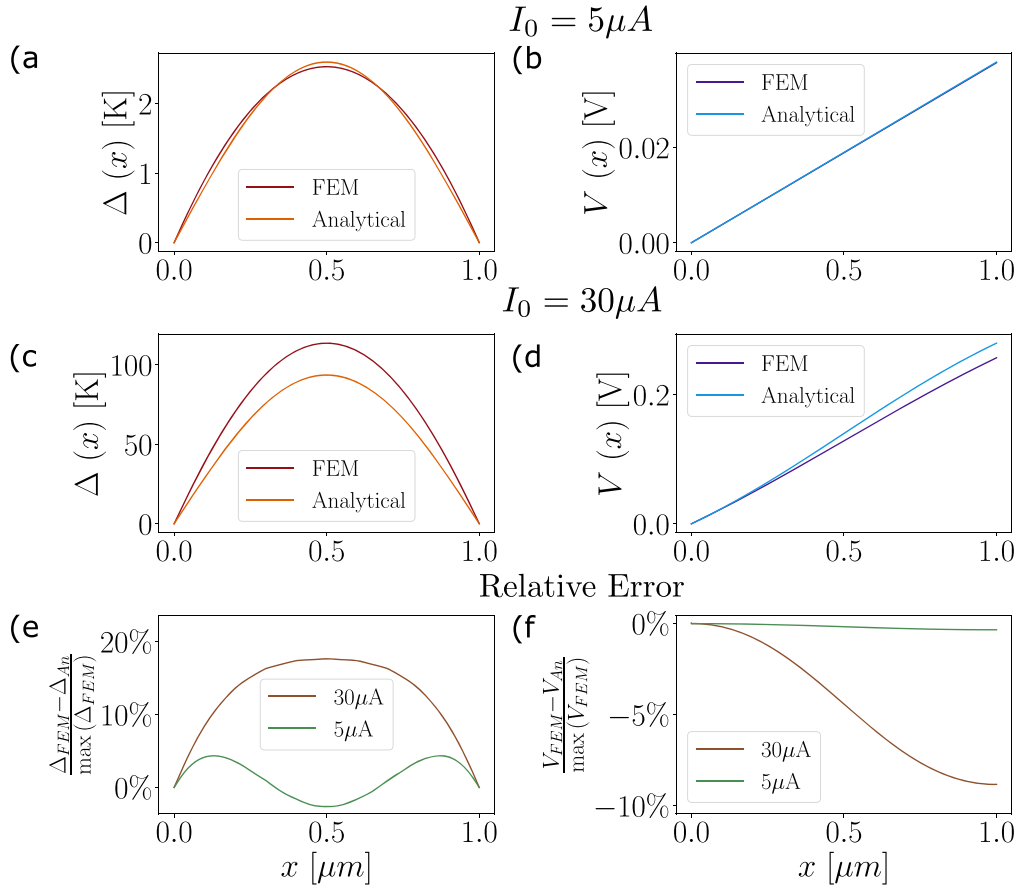
Figure 3. Particular profiles taken from figure 2 for injection currents of $5\mu A$ (a)–(b) and $30\mu A$ (c)–(d), corresponding to $\Theta = 5 \times 10^{-3}$ and $\Theta = 0.19$ respectively. From panels (a)–(b) it is clear how for $\Theta \ll 1$ the analytical and FEM models are in good agreement, especially on the voltage profile. This is the case because the $\Delta_F EM(x) - \Delta_{An}(x)$ *oscillates* along the NW, and it is integral cancels out almost exactly. When $\Theta \sim 1$, however, the effect of self-heating can no more be treated perturbatively. Panels (e)–(f) show how in this case the analytical solution would lead to an error of 20% on the maximum temperature, translating into a 9% overestimate of the voltage drop.

surface of the NW. Mathematically, this is equivalent of saying that, if we define $\hat{x}$ the direction of the NW axis, $\frac{\partial}{\partial y}T(\vec{x}, t) = \frac{\partial}{\partial z}T(\vec{x}, t) = 0$. Thus, the temperature profile $T(\vec{x}, t)$ exhibits translational invariance along y and z.

Moreover, equation (2) is linear in T. Therefore, we can rewrite the PD in terms of $\Delta(x, t) = T(x, t) - T_0$, which reads

$$\frac{\partial}{\partial t}\Delta(x, t) - \alpha\frac{\partial^2}{\partial x^2}\Delta(x, t) - \frac{1}{\gamma_J}\Delta(x, t)\sin^2(\omega t)$$
$$= \frac{1}{\gamma_J}\frac{R_0}{R'}\sin^2(\omega t), \qquad (3)$$

with the boundary conditions dictated by the experimental setup

$$\begin{cases} \Delta(0, t) = 0 \\ \Delta(L, t) = 0 \\ \Delta(x, t \to -\infty) = 0 \end{cases}. \qquad (4)$$

In equation 3 we have introduced the thermal diffusivity

$$\alpha = \frac{k}{\rho C_p} \qquad (5)$$

and the Joule heating timescale

$$\gamma_J = \frac{\rho C_p}{j_0^2 \rho'_{el}}, \qquad (6)$$

which can be interpreted as the timescale at which the NW resistance changes because of the injected current. Another timescale naturally arises from the diffusive nature of heat transport as

$$\gamma_D = \frac{L^2}{\pi^2\alpha}, \qquad (7)$$

which is the characteristic time for axial thermal processes. We note that can similarly define $\gamma_{D,r} = \frac{r^2}{\alpha}$, with r the radius of the NW, as a characteristic time for radial thermal processes. Given the high-aspect ratio of the NW we observe that $\gamma_{D,r} \ll \gamma_D$, supporting our assumption of translational invariance orthogonally to the NW axis.

While a complete and thorough derivation would be outside of the scope of this work, it is possible to show that the solution to equation (3) can be stated in the form

$$\Delta(x, t) = \int_{-\infty}^{t} d\tau \sum_{n=1}^{+\infty} U_n(t; \tau)\sin\frac{n\pi x}{L}, \qquad (8)$$

with U_n being determined by the equation

$$\frac{d}{dt}U_n + \left(\frac{n^2}{\gamma_D} - \frac{1}{\gamma_J}\sin^2(\omega t)\right)U_n = 0 \qquad \forall n. \qquad (9)$$
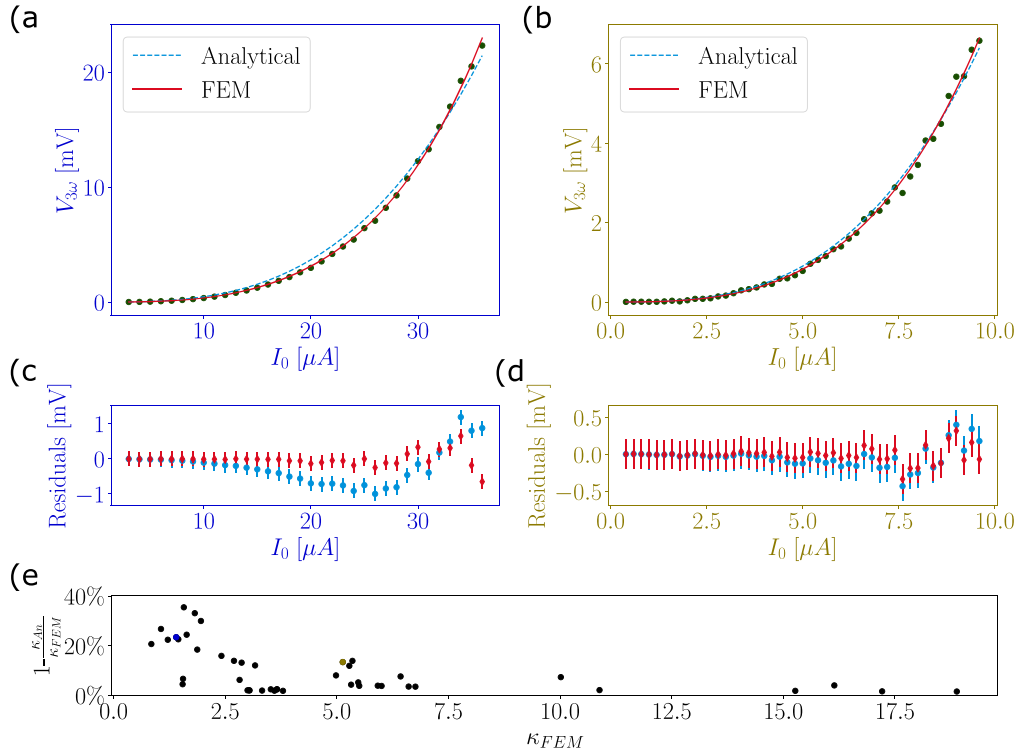
Figure 4. Analysis of the same data shown in figure 1 with both the analytical and the FEM methods. Panels (a), (c) represent the same nanostructured NW from figures 2–3, with $\kappa \approx 1 \frac{W}{mK}$ ($\kappa = 1.1 \pm 0.1 \frac{W}{mK}$ and $1.5 \pm 0.2 \frac{W}{mK}$ from the analytical and FEM models respectively). From the residuals from the best fit in panel (c) we can see how the analytical fails to correctly retrace the data, while the FEM model reproduces it more closely. Both models, however, correctly fit the experimental data for the single-crystal InAsSb NW with larger thermal conductivity ($4.7 \pm 0.3 \frac{W}{mK}$ and $5.0 \pm 0.2 \frac{W}{mK}$ for the analytical and FEM method respectively) in panels (b), (d). Panel (e) shows the relative discrepancy $\frac{\kappa_{FEM} - \kappa_{An}}{\kappa_{FEM}}$ for all experiments in the available dataset, where we can see how the analytical method *systematically underestimates* the thermal conductivity of the nanostructure. More importantly, we can see how this becomes more prominent for samples with low κ, reaching close to 40% in certain samples. The colored dots represent the samples from panels (a) and (b). Data taken as described in [2].

From equation (9) it is clear how the presence of Joule's heating and the consequent change in NW resistance causes a deviation from the simple diffusive problem. We can quantify this effect through the adimensional number

$$\Theta = \frac{\gamma_D}{\gamma_J} = j_0^2 \frac{\rho_{el}'}{\kappa} L^2. \tag{10}$$

We may also define another adimensional number

$$\Xi = \omega \gamma_D = \frac{\omega \rho C_p}{\pi^2 \kappa} L^2, \tag{11}$$

which describes the ability of the system to respond to the sinusoidally-modulated injection current.

In the regime where

$$\Theta \ll 1, \tag{12}$$

the effect of R' can be considered a perturbation of the diffusive transport. Therefore, we can consider the solution

$$\Delta(x, t) = \frac{4\Delta_0}{\pi^3} \sum_{n=0}^{+\infty} \frac{1}{(2n + 1)^3} \sin\left((2n + 1)\frac{\pi x}{L}\right)$$
$$\cdot \left(1 - \frac{\sin(2\omega t + \phi_n)}{\sqrt{1 + \cot^2 \phi_n}}\right), \tag{13}$$

where we have defined $\cot(\phi_n) = 2\frac{\omega \gamma_D}{(2n + 1)^2}$ as the cotangent of the relative phase shift of each component and

$$\Delta_0 = \frac{\gamma_D}{\gamma_J} \frac{R_0}{R'} = \frac{j_0^2 \rho_{el}}{\kappa} L^2, \tag{14}$$

which is proportional to the peak temperature for each Fourier component.

Besides the obvious relation $\Delta_0 \propto j_0^2$, is very interesting to note that $\Delta_0 \propto \frac{L^2}{k}$, which comes from the fact that both a longer NW or a smaller thermal conductivity make for a less efficient heat transfer and thus higher temperatures. A notable absent in (14) is C_p, meaning that thermodynamic information are only necessary to obtain γ, but it is only transport properties that influence the final temperature profile. We shall note that, we can now directly relate the change in NW resistance to the transport and electrical property via the relation

$$\Theta = \frac{R' \Delta_0}{R_0} \tag{15}$$

after which, as expected the condition in equation (12) simply reads

$$R' \Delta_0 \ll R_0. \tag{16}$$

It ought to be clear that, depending on the specific device, it may be challenging to fulfill this relation, especially for specimens with low κ, which are, however, the most interesting from a technological point of view, for they have the best thermoelectric performance. Particularly for those, therefore, the requirement in equation (12) clearly indicates the need for the more complete numerical treatment. It is worth mentioning here that, since the parameter Θ is related to the heat flux flowing in the nanostructure, a possible approach to force the condition in equation (12) would be to decrease the injection current. However, this approach would also cause experimental difficulties related to the decrease of the measured signals and thus a less accurate measurement of κ. For this reason, reducing the heat flux in the nanowire is not a desirable way to force the system in a regime in which the assumptions at the basis of the analytical model are valid.

If condition equation (12) is met, however, it ought to be clear that the length scale over which the NW resistance is modified with respect of R_0 because of Joule's heating is much is much larger than the NW physical length. Therefore, we may perturbatively retain only the leading term $n = 0$.

The voltage profile along the NW is given by

$$V(t) = \left(R_0 + \frac{R'}{L} \int_0^x \Delta(x', t) dx' \right) I_0 \sin(\omega t) \qquad (17)$$

thus, after trivial integration, the third harmonic for $x = L$ reads

$$V_{3\omega}(t) = -\frac{2\Theta}{\pi^4} \frac{R_0 I_0}{\sqrt{1 + 4\Xi^2}} \sin(3\omega t - \phi), \qquad (18)$$

where we have redefined the phase as $\tan(\phi) = \tan\frac{\pi}{2} - \phi_1 \approx 2\Xi$. Integrating in time in this limit, we obtain the well-known relation for the root mean square third harmonic [24]

$$V_{3\omega} = -\frac{4I_0^3 R_0 R'}{2\sqrt{2}\,\pi^4 \kappa} \frac{L}{S} \frac{1}{\sqrt{1 + 4\Xi^2}}. \qquad (19)$$

Equation (19) clearly reflects the intuition that for $\Xi \ll 1$ the system behaves quasi-statically, and temperature is able to oscillate with voltage. As the NW is driven faster, however, thermal conduction is unable to keep up with the injection current, and the temperature oscillations become damped. We also note that Ξ is the only leftover dependency upon the NW thermodynamic properties C_p. Therefore, we can deliberately choose a frequency low enough to achieve $\Xi \ll 1$, thus removing this dependency completely. This regime, as we shall see, is also advantageous for the numerical approach described in the next section, and is therefore the regime that shall uniquely discuss henceforth. The final analytical formula therefore reads

$$V_{3\omega} = -\frac{4I_0^3 R_0 R'}{2\sqrt{2}\,\pi^4 \kappa} \frac{L}{S}, \qquad (20)$$

which is the model used to fit the two curves in figure 1. However, as ought to be apparent from figure 1(b), this model cannot faithfully reproduce the experimental data. More significantly, we shall see how the difference between

figures 1(b) and (c) is that the former, where the agreement with equation (20) is poorer, represents an InAsSb NW whose nanostructure has been engineered to reduce the thermal conductivity. Considering the requirement in equation (12), it ought to be clear how this may cause the analytical model to fail by returning an underestimated value for the thermal conductivity when $\Theta \sim 1$, while still be able to reproduce the experimental data for the single-crystal InAsSb NW counterpart in figure 1(c).

3.3. Finite element treatment

In this section we shall discuss a Finite Element Modelling (FEM) approach to numerically describe physical systems in which the condition in equation (12) cannot easily be met. Our task is to solve a coupled physics problem where the set of thermoelectric partial differential equations

$$\begin{cases} \vec{j}(\vec{x}, t) = \sigma(\vec{x}, t)\vec{E}(\vec{x}, t) - S_e \sigma(\vec{x}, t)\vec{\nabla}T(\vec{x}, t) \\ \vec{\Phi}(\vec{x}, t) = \Pi\vec{j}(\vec{x}, t) - \kappa\vec{\nabla}T(\vec{x}, t) \end{cases}, \qquad (21)$$

must be solved together with the heat equation

$$\rho C_p \frac{\partial}{\partial t} T(\vec{x}, t) = -\vec{\nabla} \cdot \vec{\Phi}(\vec{x}, t) + \dot{q}(\vec{x}, t) \qquad (22)$$

to obtain the correct $V_{3\omega}$ given the appropriate boundary conditions. In equation (22) we have used $\dot{q}(\vec{x}, t)$ to indicate the local heat generation in the specimen.

It is possible to prove that direct coupling of $\vec{j}$ and $\vec{\Phi}$ because of the Seebeck S_e and Peltier $\Pi = TS_e$ coefficients are usually negligible because of the injected current and the comparatively smaller temperature gradients [13, 25, 33, 34]. Thus equation (21) greatly simplifies to

$$\begin{cases} \vec{j}(\vec{x}, t) = \sigma(\vec{x}, t)\vec{E}(\vec{x}, t) \\ \vec{\Phi}(\vec{x}, t) = \kappa\vec{\nabla}T(\vec{x}, t) \end{cases}. \qquad (23)$$

This, together with the microscopic definition of Joule's heating $\dot{q}(\vec{x}, t) = \vec{j}(\vec{x}, t) \cdot \vec{E}(\vec{x}, t)$, allows us to rewrite equation (22) as

$$\rho C_p \frac{\partial}{\partial t} \Delta(\vec{x}, t) = -\kappa\nabla^2\Delta(\vec{x}, t) + \vec{j}(\vec{x}, t) \cdot \vec{E}(\vec{x}, t), \qquad (24)$$

where we have once again employed the linearity of equation (22) to define $\Delta(\vec{x}, t) = T(\vec{x}, t) - T_0$ for consistency with the above discussion.

It is easy to see that this formulation is equivalent to equation (2) in the microscopic formalism.

We can now consider the effect of Joule's heating through the definition

$$\sigma(\vec{x}, t) = \frac{1}{R}\frac{L}{S} = \frac{1}{R_0 + R'\Delta(\vec{x}, t)}\frac{L}{S}. \qquad (25)$$

If we now consider the regime where $\Xi \ll 1$, the system has plenty of time to follow the changes in $\vec{j}(t)$, and thus behaves quasi-statically. Hence

$$\frac{\partial}{\partial t}\Delta(\vec{x}, t) \underset{\Xi \to 0}{\longrightarrow} 0. \qquad (26)$$

Therefore, the heat equation reads

$$\kappa \nabla^2 \Delta(\vec{x}, t) = \vec{j}(\vec{x}, t) \cdot \vec{E}(\vec{x}, t), \tag{27}$$

which, combined with equation (25), becomes

$$\kappa \nabla^2 \Delta(\vec{x}, t) = -\frac{|\vec{\nabla} V(\vec{x}, t)|^2}{R_0 + R' \Delta(\vec{x}, t)} \frac{L}{S}, \tag{28}$$

where, for notational convenience in the subsequent paragraphs, we have simply written the electric field inside the specimen as $\vec{E}(\vec{x}, t) = -\vec{\nabla} V(\vec{x}, t)$. It is worth stressing that L, S, R_0 and R' are all quantities which can be separately measured, thus the only unknown parameter, to be obtained through fitting of experimental data, in equation (28) is the thermal conductivity κ.

A full definition of the problem, however, is still lacking a way to compute the local electrical potential. This could be achieved through the charge continuity equation. Since equation (28) describes a stationary solution, this takes the form $\vec{\nabla} \cdot \vec{j}(\vec{x}, t) = 0$. Together with the first equation in equations (23), we can thus write

$$\vec{\nabla} \cdot (\sigma(\vec{x}, t) \vec{\nabla} V(\vec{x}, t)) = 0, \tag{29}$$

which merely states that no charge is accumulating inside the specimen. Equations (28) and (29) together represent the strong formulation of the problem. It is worth mentioning that the need for a system of coupled equations arises due to the fact that the electrical resistance of the specimen depends on the temperature through the temperature resistance coefficient R. Thus, a precise solution for the problem under consideration requires to solve the heat and electrical transport equations by coupling them rather than considering the Joule heating effect as a fixed heat source for the heat transport equation and solely solve the latter. In order to properly solve it through the Finite Element Method [35–40], however, we have to derive its weak definition. A detailed description of the steps followed and selected would be out of the scope of this work, and it is detailed in the supplementary information in appendix section C.

Once the coupled physics problem has been correctly defined, the last thing to impose before being able to implement a solution is to impose the correct boundary conditions. The same argument of translational invariance holds for the FEM model as well. Therefore, NW temperature still follows the boundary conditions in equation (4) This, however, is no more enough for we are dealing with a system of two coupled equations. Since equation (29) if formally a second-order ODE we shall thus impose two more boundary conditions. The first one can be enforced experimentally by tying one of the external contacts to ground, while the last one comes down to simply requiring that the current forced through the specimen at each instant in time amounts to the injection current $I(t)$. Therefore, this translates to

$$\begin{cases} V(0, t) = 0 \\ \int_{x=L} \vec{j}(\vec{x}, t) \cdot \vec{dS} = I_0 \sin(\omega t) \end{cases}, \tag{30}$$

where $\int_{x=L}$ refers to the surface in contact with the non-grounded outer metal pad. Because of equation (29), the

second condition in (30) automatically implies that

$$\oint \vec{j}(\vec{x}, t) \cdot \vec{dS} = 0, \tag{31}$$

so that all the injected current is always flowing out of the NW and there is no charge accumulation inside the specimen.

Finally, we shall note that, thanks to the properties of the problem, both the temperature and voltage profile will possess translational symmetry in the plane orthogonal to the NW axis. Thus, we can simply write

$$\vec{j}(t) = \frac{I_0}{S} \sin(\omega t) \hat{x}. \tag{32}$$

Nevertheless, in the present paragraphs the 3D notation will still be employed because the resolution will take place over a 3D mesh, as, each NW was modeled as an hexagonal prism with the corresponding measured length and diameter.

Finally, we ought to point out that the second condition in equation (30) is not a Dirichlet condition. Consequently, its FEM implementation does require some additional work, which is reported appendix ?, where it is shown that, because of the particular properties of our problem, this last condition is mathematically equivalent to a Von Neumann boundary condition.

4. Discussion

4.1. Comparison between the FEM and analytical results

4.1.1. $\Theta \ll 1$. equations (28)–(29), together with the appropriate boundary conditions, completely define the 3ω problem as long as the experimental conditions fulfill $\Xi \ll 1$. It is interesting, however, to consider the FEM model in the regime $\Theta \ll 1$. In this case, once again, we can consider Joule's heating as a perturbation of the temperature profile, which reads, at first order

$$\Delta(\vec{x}, t) = \frac{\Delta_0}{2} \frac{x(L - x)}{L^2} \sin \omega t, \tag{33}$$

which is the well-known parabolic solution to the heat equation with uniform heat generation ($O(\Theta)$). This is in contrast with the sinusoidal profile arising from the Fourier expansion in the analytical treatment. Moreover, if we consider the total change in NW resistance

$$\delta R = R - R_0 = \frac{R'}{L} \int_0^x \Delta(x', t) dx', \tag{34}$$

is the similar for both models. In particular, $\delta R_{An} = \frac{8}{\pi^4} R' \Delta_0 \approx 0.082 R' \Delta_0$, while $\delta R_{FEM} = \frac{1}{12} R' \Delta_0 \approx 0.083 R' \Delta_0$. Therefore, the error on the voltage drop across the NW given by equation (17), and thus equation (20), is of order $1 - \frac{\pi^4}{96} \approx 1\%$. Thus, $V_{3\omega}$ remains largely the same as long as $\Theta \ll 1$ and we can neglect the *non-homogeneous* heating effect created by a change in local temperature. This shall appear even more clearly during the discussion of figure 3. We shall note that if *all* the terms in the infinite series in

equation (13) were used, instead of only $n = 0$, both models would predict $\delta R = \frac{1}{12} R' \Delta_0$, as ought to be expected.

4.1.2. $\Theta \sim 1$. A comparison between the analytical and FEM models in the regime where $\Theta \sim 1$ is presented in figure 2 for various injection currents. For the sake of presenting a meaningful example, the simulations have been performed with the parameters of one of the InAsSb NWs from the dataset discussed in section 4.2. In particular, we chose the device used to measure figures 1(a) and 4(a). The relevant parameters are: 1 μm length, 35 nm diameter, and $\kappa = 1.5 \frac{W}{mK}$. From figures 2(a)–(b), we can see the qualitative similarity of the two models hitherto discussed. It is clear, however, that the two have a significant discrepancy in the peak temperature, especially for higher currents. Nevertheless, this regime is the most useful from an experimental point of view, as the stronger non-linearity of the NW response allows for better signal-to-noise ratio. The aforementioned disagreement between the two models is caused by the low value of κ of the NW chosen as an example, whose engineered superlattice lowers thermal transport by an order of magnitude with respect to the respective homogeneous InAs crystal. This drop in thermal conductivity means that it becomes challenging to fulfil equation (12) in typical experimental conditions, with the parameters reaching $\Theta = 0.33$ for the higher temperature. Therefore, it becomes clear that the effects of self-heating and the resulting gradients in electrical conductivity can no more be neglected, and must be taken into account in an FEM model. Most importantly, from equation (17) we can see how the underestimate in the NW temperature profile results in an overestimate $V(x)$, and therefore of $V_{3\omega}$.

This discrepancy is highlighted in figure 3, which shows a direct comparison between the two models for injection currents of $5 \mu A$ (figures 3(a)–(b)) and $30 \mu A$ (figure 3(c)–(d)), corresponding to $\Theta = 5 \times 10^{-3}$ and $\Theta = 0.19$ respectively. Echoing the previous remarks, we shall see how for the lower injection current we fulfil $\Theta \ll 1$, and thus the error on the temperature remains bound to a few percent. Moreover, as clear from figure 3(a), $\Delta_F EM(x) - \Delta_{An}(x)$ *oscillates* along the NW, and it is integral cancels out almost exactly. As we can clearly see from figure 3(e), when $\Theta \sim 1$ taking the local effect of Joule's heating into account causes a discrepancy up to 20% between the analytical 3ω approach and the (more accurate) Finite Element modelling. In turn, this also causes a discrepancy in the voltage profile. This is even more significant than the $\Theta \ll 1$, as $\Delta_F EM(x) - \Delta_{An}(x) > 0$ along the whole NW. Thus, the error on the voltage accumulates rather than cancelling out, which manifests in an *overestimate* of the voltage drop of 9%. Considering equation (20), it is clear how therefore the naive analysis would lead to an *underestimate* of the NW thermal conductivity, thus highlighting the requirement for a self-consistent FEM modelling the thermal and electrical profiles in nanostructures, especially those engineered to lower their thermal conductivity.

4.2. Extracting κ from experimental data

Finally, we shall compare the two methods on an actual experimental dataset, taken as described in [2], where we demonstrate a drastic reduction in thermal conductivity in InAsSb NWs thanks to a twinning superlattice crystal structure. This lends itself particularly well to the task, for it contains 3ω measurements for a wide variety of thermal conductivities, while maintaining similar physical and electrical properties. For the finite element modeling, the calculations are performed within a Python code employing the FEniCS package [41] and the solution is directly exploited to fit experimental data within the same framework consistently (see supplementary info sections B, C for more detailed information). Figures 4(a)–(b) show the same $V_{3\omega}(I_0)$ curves from figure 1, but now with also the FEM fit. Figures 4(a), (c) show the same nanostructured NW from figures 2–3, while figures 4(b), (d) represent a single-crystal InAsSb NW with larger thermal conductivity. It ought to be clear how the FEM model is in far better agreement with the experimental datasets than equation (20). This appears evident also from the reported residuals, where the analytical model, unlike the FEM simulations, clearly shows an oscillating trend in figure 4(c). Moreover, while the two models give a similar estimate of κ for the device in panel (b), $4.7 \pm 0.3 \frac{W}{mK}$ and $5.0 \pm 0.2 \frac{W}{mK}$ for the analytical and FEM method respectively, the two are significantly different in the case of the nanostructured NW in panel (a). Namely, equation (20) not only clearly does not fit well the data, but estimates $\kappa = 1.1 \pm 0.1 \frac{W}{mK}$. The FEM model, on the other hand, returns a value of $1.5 \pm 0.2 \frac{W}{mK}$, amounting to an *underestimate* of almost 30%. The explanation for this phenomenon ought to be clear from the theory, as a reduction in κ implies an increase in Θ, which may push the experimental conditions outside the range of validity of equation (20). This trend is shown even more clearly in 4(e), where we can see how such an underestimate is common for all the low-κ devices. We can quantify this by considering the relative discrepancy $\frac{\kappa_{FEM} - \kappa_{An}}{\kappa_{FEM}}$, which we can see being no less than 25% in almost all nanostructured NWs, reaching close to 40% in some occasions. More importantly, the nature of this error is systematic because of the break down of the main assumption of the underlying theoretical result, and thus can only be corrected with the use of a more suitable model. Lastly, we shall stress how the naive application of the 3ω-method in low-κ specimens systematically leads to measuring an *lower* thermal conductivity. This is of crucial importance in phonon-engineered or nanostructured systems for thermal applications, where the effect of the nano-engineering may be erroneously overestimated, which may in turn lead to an over-inflation of the predicted thermoelectric performance.

5. Conclusion

This work clearly shows the need for accurate numerical simulations, such as Finite Element Modelling, when extracting thermal conductivity of nanostructures with low κ with the

3ω-method. In particular, we have shown how the application of the analytical results, which are routinely applied in measurements of state-of-the-art high-aspect-ratio nanostructures, particularly semiconducting NWs, can lead to a significant systematic error on the extracted thermal conductivity. In particular, we shall stress how this is a systematic *underestimate* of κ, which we have shown in experimental data to reach almost 30%. Specifically, we have identified the adimensional parameter Θ describing the regime in which the analytical approach is effective (i.e. $\Theta \ll 1$). When this relation is not respected, then resorting to the finite element modelling approach to extract κ is crucial for the 3ω technique to be effective.

This remark is of particular importance since low-κ nanostructures are the devices which are the most interesting from the technological point of view of thermoelectric application. The stride to lower the thermal through phonon-engineering and nanotechnology, on the pursuit of higher thermoelectric figures of merit, may therefore risk to be artificially inflated by the naive application of a methods whose very assumptions require thermal conductivity to be *large enough* to treat thermal transport perturbatively.

In this work, we also propose a more robust and mathematically-sound approach based on the numerical solution of the heat equation via Finite Element Modelling. This relaxes the low-κ assumptions, and thus can more precisely assess the thermal transport, and thus thermoelectric, performance of a nanostructure, more reliably extracting its thermal conductivity. We invite other groups developing low thermal conductivity materials to adopt the method described in this work in order to assess its robustness deriving from the mathematical framework it has been developed on and to more precisely measure the thermal conductivity of their samples to establish new records in high-performance thermoelectric nanomaterials.

Acknowledgments

Data availability statement

All data that support the findings of this study are included within the article (and any supplementary files).

ORCID iDs

Domenic Prete https://orcid.org/0000-0002-8044-0924

References

[1] Prete D, Demontis V, Zannier V, Rodriguez-Douton M J, Guazzelli L, Beltram F, Sorba L and Rossella F 2021 Impact of electrostatic doping on carrier concentration and mobility in InAs nanowires *Nanotechnology* **32** 145204

[2] Peri L, Prete D, Demontis V, Zannier V, Rossi F, Sorba L, Beltram F and Rossella F 2022 Giant reduction of thermal conductivity and enhancement of thermoelectric performance in twinning superlattice inassb nanowires *Nano Energy* **103** 107700

[3] Roddaro S, Ercolani D, Safeen M A, Suomalainen S, Rossella F, Giazotto F, Sorba L and Beltram F 2013 Giant thermovoltage in single inas nanowire field-effect transistors *Nano Lett.* **13** 3638–42

[4] Chen Z G, Han G, Yang L, Cheng L and Zou J 2012 Nanostructured thermoelectric materials: current research and future challenge *Progress Nat. Sci.: Mater. Int.* **22** 535–49

[5] Chen R, Lee J, Lee W and Li D 2019 Thermoelectrics of nanowires *Chem. Rev.* **115** 9260–302

[6] Blanc C, Rajabpour A, Volz S, Fournier T and Bourgeois O 2013 Phonon heat conduction in corrugated silicon nanowires below the casimir limit *Appl. Phys. Lett.* **103** 043109

[7] Nakamura Y 2018 Nanostructure design for drastic reduction of thermal conductivity while preserving high electrical conductivity *Sci. Technol. Adv. Mater.* **19** 31–43

[8] Casimir H 1938 Note on the conduction of heat in crystals *Physica* **5** 495–500

[9] Zabek D and Morini F 2019 Solid state generators and energy harvesters for waste heat recovery and thermal energy harvesting *Thermal Sci. Eng. Progress* **9** 235–47

[10] Bos J W G, Zandbergen H W, Lee M H, Ong N P and Cava R J 2007 Structures and thermoelectric properties of the infinitely adaptive series $(Bi_2)_m(Bi_2Te_3)_n$ *Phys. Rev.* B **75** 195203

[11] Chen X K and Chen K Q 2020 Thermal transport of carbon nanomaterials *J. Phys. Condens. Matter* **32** 153002

[12] Jia P Z, Xie J P, Chen X K, Zhang Y, Yu X, Zeng Y J, Xie Z X, Deng Y X and Zhou W X 2022 Recent progress of two-dimensional heterostructures for thermoelectric applications *J. Phys. Condens. Matter* **35** 073001

[13] Cahill D G 1990 Thermal conductivity measurement from 30 to 750 K: the 3ω method *Rev. Sci. Instrum.* **61** 802–8

[14] Rossella F, Pennelli G and Roddaro S 2018 Measurement of the thermoelectric properties of individual nanostructures *Semiconductors and Semimetals* vol 98 (New York: Academic) pp 409–44

[15] Bhardwaj R G and Khare N 2022 Review: 3-ω technique for thermal conductivity measurement—contemporary and advancement in its methodology *International Journal of Thermophysics volume* **43** 139

[16] Wang H and Sen M 2009 Analysis of the 3-omega method for thermal conductivity measurement *Int. J. Heat Mass Transfer* **52** 2102–9

[17] Jacquot A, Vollmer F, Bayer B, Jaegle M, Ebling D G and Böttner H 2010 Thermal conductivity measurements on challenging samples by the 3 omega method *J. Electron. Mater.* **39** 1621–6

[18] Hasegawa Y, Murata M, Tsunemi F, Saito Y, Shirota K, Komine T, Dames C and Garay J E 2013 Thermal conductivity of an individual bismuth nanowire covered with a quartz template using a 3-omega technique *J. Electron. Mater.* **42** 2048–55

[19] Yazji S, Hoffman E A, Ercolani D, Rossella F, Pitanti A, Cavalli A, Roddaro S, Abstreiter G, Sorba L and Zardo I 2015 Complete thermoelectric benchmarking of individual InSb nanowires using combined micro-Raman and electric transport analysis *Nano Res.* **8** 4048–60

[20] Zhu J, Wu X, Lattery D M, Zheng W and Wang X 2017 The ultrafast laser pump-probe technique for thermal characterization of materials with micro/nanostructures *Nanoscale Microscale Thermophys. Eng.* **21** 177–98

[21] Weathers A, Moore A L, Pettes M T, Salta D, Kim J, Dick K, Samuelson L, Linke H, Caroff P and Shi L 2011 Phonon transport and thermoelectricity in defect-engineered InAs

nanowires *Materials Research Society Symp. Proc.* vol 1404 (Springer) pp 44–51

[22] Roddaro S, Ercolani D, Safeen M A, Rossella F, Piazza V, Giazotto F, Sorba L and Beltram F 2013 Large thermal biasing of individual gated nanostructures *Nano Research* **7** 579–87

[23] Prete D, Erdman P A, Demontis V, Zannier V, Ercolani D, Sorba L, Beltram F, Rossella F, Taddei F and Roddaro S 2019 Thermoelectric conversion at 30 k in InAs/InP nanowire quantum dots *Nano Lett.* **19** 3033–9

[24] Lu L, Yi W and Zhang D L 2001 3 Ω method for specific heat and thermal conductivity measurements *Rev. Sci. Instrum.* **72** 2996–3003

[25] Pennelli G, Dimaggio E and Macucci M 2018 Note: improvement of the 3ω thermal conductivity measurement technique for its application at the nanoscale *The Review of Scientific Instruments* **89** 016104

[26] Ramu A T and Bowers J E 2012 Analysis of the '3-omega' method for substrates and thick films of anisotropic thermal conductivity *J. Appl. Phys.* **112** 043516

[27] Al-Khudary N, Cresson P Y, Orlic Y, Coquet P, Pernod P and Lasri T 2014 Measurement of the thermal conductivity of polydimethylsiloxane polymer using the three omega method *Key Engineering Materials* Measurement Technology and Intelligent Instruments XI **613** pp 259–66

[28] Rodrigo O and Bertrand G 2022 Radial thermal conductivity of a pan type carbon fiber using the 3 omega method *Int. J. Therm. Sci.* **172** 107321

[29] Guermoudi A A, Cresson P Y, Ouldabbes A, Boussatour G and Lasri T 2021 Thermal conductivity and interfacial effect of parylene c thin film using the 3-omega method *J. Therm. Anal. Calorim.* **145** 1–12

[30] Mion C, Muth J, Preble E A and Hanser D 2006 Thermal conductivity, dislocation density and gan device design *Superlattices Microstruct.* **40** 338–42

[31] Swinkels M Y, Van Delft M R, Oliveira D S, Cavalli A, Zardo I, Van Der Heijden R W and Bakkers E P 2015 Diameter dependence of the thermal conductivity of InAs nanowires *Nanotechnology* **26** 38

[32] Cahill D G, Watson S K and Pohl R O 1992 Lower limit to the thermal conductivity of disordered crystals *Phys. Rev.* B **46** 6131–40

[33] Pennelli G, Nannini A and Macucci M 2014 Indirect measurement of thermal conductivity in silicon nanowires *J. Appl. Phys.* **115** 084507

[34] Rocci M, Demontis V, Prete D, Ercolani D, Sorba L, Beltram F, Pennelli G, Roddaro S and Rossella F 2018 Suspended InAs nanowire-based devices for thermal conductivity measurement using the 3ω method *J. Mater. Eng. Perform.* **27** 6299–305

[35] Kirby R C and Logg A 2012 Finite element variational forms *Automated Solution of Differential Equations by the Finite Element Method* (Berlin: Springer) 133–40

[36] Kirby R C and Logg A 2012 The finite element method *Automated Solution of Differential Equations by the Finite Element Method* (Berlin: Springer) 77–94

[37] Kirby R C and Logg A 2006 A compiler for variational forms *ACM Trans. Math. Softw.* **32** 417–44

[38] Logg A, Mardal K A and Wells G N 2012 Automated solution of differential equations by the finite element method *Lect. Notes Comput. Sci. Eng.* **84 LNCSE** 1–736

[39] Geuzaine C and Remacle J F 2009 Gmsh: a 3D finite element mesh generator with built-in pre- and post-processing facilities *Int. J. Numer. Methods Eng.* **79** 1309–31

[40] 2006 Finite Element Procedures Second Edition Bathe Finite Element Procedures Klaus-Jürgen Bathe Second Edition

[41] Alnaes M S, Blechta J, Hake J, Johansson A, Kehlet B, Logg A, Richardson C, Ring J, Rognes M E and Wells G N 2015 The FEniCS project version 1.5 *Archive Num. Software* **3** 100